Responses to the Reviewers

We thank both the referees for carefully reviewing our manuscript and providing suggestions to improve the clarity and quality of the paper.

The figures only appeared in the responses are named as 'R+Number' (e.g., figure R1).

Reviewer # 1

Comments 1: There needs to be some discussion on the influences of biomass burning aerosols in the atmosphere. They are also a primary source of carbonaceous aerosols and may impact aerosol-PBL interactions very similar to urban/industrial pollution.

Response: Yes, fossil fuel combustion and biomass burning are the main sources releasing carbon aerosols into the atmosphere. The biomass burning aerosols, which are characterized by large amount of fine mode particles and comparatively low single scattering albedo, contribute significantly to the earth's radiation balance, consequently changing the atmospheric thermodynamic stability, and thereby cloud formation. The combination of pollutants from biomass burning and industrial emissions in eastern China results in extreme air pollution around the surface via aerosol-PBL interactions (Ding et al., 2013). Here, contribution of biomass burning to carbonaceous aerosols over the GZP was discussed by employing the aerosol optical depth and the fire hot spot data derived from MODIS, and the attenuation coefficients acquired by an aethalometer (Model AE-31) at the Xi'an site (108.97°E, 34.43°N).

Figure R1 shows the spatial distribution of daytime fire counts in summer during 2002–2014 over mainland China based on AQUA/MODIS collection 6 active fire product. Clearly, the most intense biomass burning activity was detected in eastern and northern China plain. The open agricultural fires occurred in the GZP were less intense than those regions. However, the highest summertime

elemental carbon (EC) and organic carbon (OC) concentrations were observed at Xi'an and Chongqin among 14 of China's large cities (Cao et al., 2012), suggesting that the biomass burning is not the main source of carbonaceous aerosols over the GZP. Besides, AOD values at 550 nm were regressed against the fire counts over the GZP (Fig. R2). The result showed the biomass burning activities have an insignificant positive impact on the AOD (p=0.25), consistent with that reported by L. Wang et al. (2015).

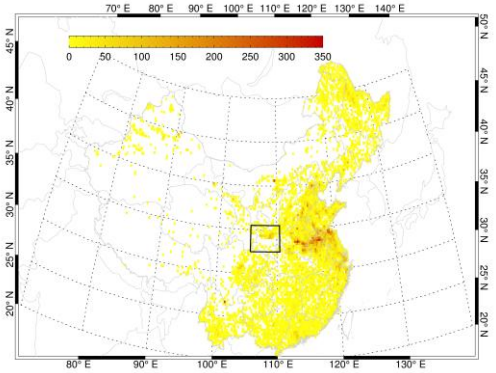

Fig. R1. Spatial distribution of daytime fire counts in summer during 2002–2014 over mainland China based on AQUA/MODIS Collection 6 Active Fire Product. The black box shows the Guan-Zhong Plain.

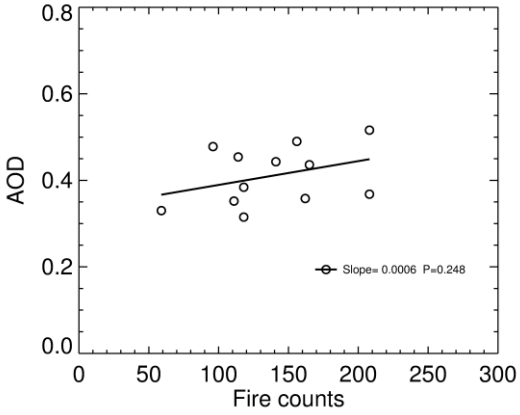

Fig. R2. Scatterplots of AOD as a function of the fire counts over the Guan-Zhong Plain

To further explore the major source of the carbonaceous aerosols in the GZP, the absorption coefficients of carbonaceous aerosols at 7 wavelengths (i.e., 370, 470, 520, 590, 660, 880 and 950 nm) are estimated by using the attenuation coefficients acquired by an aethalometer (Model AE-31) at the Xi'an site (108.97°E, 34.43°N) following the method proposed by Aruna et al. (2013). The spectral dependence of the absorption coefficients, namely, the absorption wavelength exponent (α), crucially depends on the source of the aerosols (Aruna et al., 2013; Weingartner et al., 2003). The value of α is below or close to 1.0 for aerosols from fossil fuel combustion, between 1.5 and 3 for biomass burning aerosols, and between 2 and 3 for dust particles (Sotogarcía, et al., 2011; Aruna et al., 2013 and references therein).

The value of α can be determined by fitting a power law to the absorption coefficients data：

$\sigma_{\lambda} = \beta\lambda^{-\alpha}$,

where σ_{λ} is the spectrally dependent absorption coefficients, β is a constant, and λ is the light wavelength.

As shown in Fig. R3, the value of α derived from the AE-31 at Xi'an is 0.82 and 0.86 in summer of 2011 and 2012, respectively, indicating that the substantial black carbon at Xi'an is predominantly from fossil fuel. It is noted that the α in winter (the value is 1.15) at Xi'an is much higher than that in summer, which can be explained by abundant domestic biomass combustion for residential heating in winter (Cao et al., 2012; Huang et al., 2014).

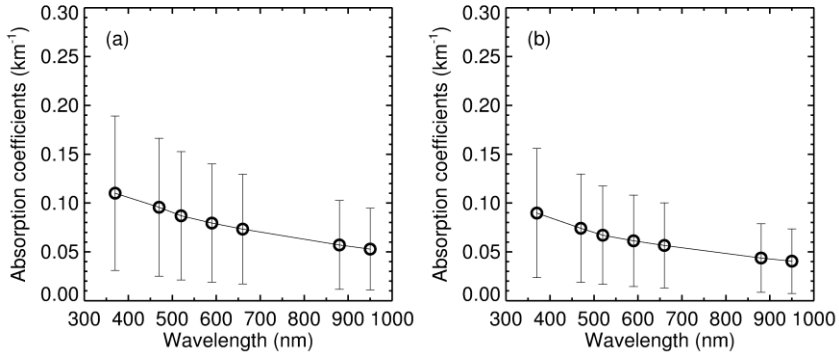

Fig. R3. Spectral values of the absorption coefficients measured by AE-31 in summer of (a) 2011 and (b) 2012 at Xi'an.

Overall, the results demonstrate that the biomass burning aerosols over the GZP have an insignificant influence on both the concentration of BC and the total column aerosol optical depth in summer. Thus, we made a little change and following sentences was added in the revised manuscript.

Changes in manuscript: Page 2, line 13-15, text was added as: "Together with fossil fuel combustion, biomass burning is the main source releasing absorbing aerosols into the atmosphere. Besides the urban/industrial pollution, Zhang et al. (2008) and Tesfaye et al. (2014) demonstrated that the biomass burning aerosols have an important impact on the evolution of PBL as well."

Comments 2: More discussion on PBL dynamics should be included as well (e.g. Page 6 Line 24)

Response: We have added the following discussion on PBL dynamics in the revised manuscript.

Changes in manuscript: Page 2, line 18-24, text was added as: "Through scattering and absorption of solar radiation, atmospheric aerosols reduce net surface shortwave radiation (SSR) and thus induce surface cooling. The decreased net SSR reduces sensible heat fluxes (Zhang et al., 2008), which leads to weakened surface buoyancy fluxes (Tesfaye et al., 2014). Moreover, black carbon aerosols absorb solar radiation in the visible wavelengths and consequently warm up and stabilize the atmosphere. The changes in atmospheric radiative heating rate and atmospheric stability depend on the vertical distribution of aerosols (Gonçalves et al., 2015). If the absorbing aerosols are confined to the PBL, they may incur or strengthen a temperature inversion below the entrainment zone, leading to the suppression of vertical motion and to a shallower PBL (Barbaro et al., 2013). "

Page 8, line 4-9, text was added as: "The parameterization schemes developed by Xia et al. (2007) were used to quantitatively estimate the aerosol-induced changes in the net SSR, namely the aerosol direct radiative forcing (ADRF) at the surface, at Xi'an by using the AOD retrievals from the MFRSR, the MODIS surface albedo products (MCD43B3), and the global shortwave radiation (SWR)

measured by Kipp-Zonen CMP21 from June 2013 to August 2014. The diurnal variation of the ADRF in summer at Xi'an is shown in Fig. S1. The mean diurnal ADRF is -35.7 W m^{-2} for the global SWR at the surface in summer. And, the ADRF during the daytime showed very large negative values, indicating weakened surface buoyancy fluxes and decreased PBLH (Zhang et al., 2008; Tesfaye et al., 2014)."

References

Aruna, K., Kumar, T. V., Rao, D. N., Murthy, B. V., Babu, S. S., Moorthy, K. K.: Black carbon aerosols in a tropical semi-urban coastal environment: Effects of boundary layer dynamics and long range transport. J. Atmos. Sol-Terr. Phys., 104(5),116-125, doi: 10.1016/j.jastp.2013.08.020,2013.

Barbaro, E., Arellano, V. G., Krol, M. C., Holtslag, A. A.: Impacts of aerosol shortwave radiation absorption on the dynamics of an idealized convective atmospheric boundary layer, Bound-Lay. Meteorol., 148(1), 31-49, doi:10.1007/s10546-013-9800-7, 2013.

Cao, J. J., Shen, Z. X., Chow, J. C., Watson, J. G., Lee, S. C., Tie, X. X., Ho, K. F., Wang, G. H., Han, Y. M.: Winter and summer PM2.5 chemical compositions in fourteen Chinese cities, J. Air. Waste. Manag. Assoc., 62(10),1214-1226, doi:10.1080/10962247.2012.701193, 2012.

Ding, A. J., Fu, C. B., Yang, X. Q., Sun, J. N., Peteja, T., Kerminen, V. M., Wang, T., Xie, Y. N., Herrmann, E., Zheng, L. F., Nie, W., Liu, Q., Wei, X. L., and Kulmala, M.: Intense atmospheric pollution modifies weather: a case of mixed biomass burning with fossil fuel combustion pollution in eastern China, Atmos. Chem. Phys., 13, 10545–10554,20 doi:10.5194/acp-13-10545-2013, 2013.

Gonçalves, W. A., Machado, L. A., and Kirstetter P. E.: Influence of biomass aerosol on precipitation over the Central Amazon: an observational study, Atmos. Chem. Phys., 15, 6789–6800, doi:10.5194/acp-15-6789-2015, 2015.

Huang, R. J., Zhang, Y., Bozzetti, C., Ho, K. F., Cao, J. J., Han, Y. M., Daellenbach, K. R., Slowik, J. G., Platt, S. M.,Canonaco, F., Zotter, P., Wolf, R., Pieber, S. M., Bruns, E. A., Crippa, M., Ciarelli, G., Piazzalunga, A.,Schwikowski, M., Abbaszade, G., Schnelle-Kreis, J., Zimmermann, R., An, Z. S., Szidat, S.,

Baltensperger, U., Haddad I. E., and Prévôt A. S.: High secondary aerosol contribution to particulate pollution during haze events in China, Nature,514, 218–222, doi:10.1038/nature13774, 2014.

Sotogarcía, L. L., Andreae, M. O., Andreae, T. W., Artaxo, P., Maenhaut, W., Kirchstetter, T., Novakov, T., Chow, J. C., Mayolbracero, O. L.: Evaluation of the carbon content of aerosols from the burning of biomass in the Brazilian Amazon using thermal, optical and thermal-optical analysis methods, Atmos. Chem. Phys., 11, 4425-4444 , doi:10.5194/acp-11-4425-2011, 2011.

Tesfaye, M., Botai, J., Sivakumar, V., Tsidu, G. M.: Simulation of biomass burning aerosols mass distributions and their direct and semi-direct effects over south africa using a regional climate model, Meteorl. Atmos. Phys., 125(3), 177-195, doi:10.1007/s00703-014-0328-2, 2014.

Wang, L. L., Xin, J. Y., Li, X. R., Wang, Y. S.: The variability of biomass burning and its influence on regional aerosol properties during the wheat harvest season in North China, Atmos. Res., 157,153-163, doi: 10.1016/j.atmosres.2015.01.009,2015.

Weingartner, E., Saathoff, H., Schnaiter, M., Streit, N., Bitnar, B., Baltensperger, U.: Absorption of light by soot particles: determination of the absorption coefficient by means of aethalometers, J. Aeros. Sci., 34(10), 1445-1463, doi:10.1016/S0021-8502(03)00359-8, 2003.

Xia, X. A., Li, Z. Q., Holben, B., Wang, P. C., Eck, T., Chen, H. B., Cribb, M., Zhao, Y. X.: Aerosol optical properties and radiative effects in the Yangtze Delta region of China, J. Geophys. Res., 112, d22s12, doi:10.1029/2007JD008859, 2007.

Zhang, Y., Fu, R., Yu, H. B., Dickinson, R. E., Juarez, R. N., Chin, M., Wang, H.: A regional climate model study of how biomass burning aerosol impacts land-atmosphere interactions over the Amazon, J. Geophys. Res., 113, d14s15, doi:10.1029/2007jd009449, 2008.

Reviewer # 2

General comments:

Aerosol-PBL feedback has been found to play very important roles in enhancing surface air pollution in many regions. Existing studies, especially some latest modeling works, revealed the mechanism and key processes of this kind of feedback. From an obvious opposite long-term trends in aerosol between lower PBL and upper PBL, this study provides additional observational testimony from satellite retrievals to show how important this feedback is in China. In general, this paper was well-written and the main results certainly will help improve the current understanding of air pollutant in China and many other regions.

Based on comprehensive data analysis and validation using various data (e.g. satellite and ground-based remote sensing data, ground based in-situ measurements etc.), this study provides solid evidence to show the opposite trends in aerosols between lower and upper PBL in Guanzhong Plain and other regions in China. The method of topography-based calculation of vertical trend AOD is very unique. However, understanding a direct linkage between the opposite trend in upper and lower altitudes with the aerosol-PBL feedback needs more clarifications.

Specific Comments 1: **For a reader who is not familiar with the aerosol-PBL feedback, maybe it is difficult to directly link the two points. The feedback scheme has been already well-established in previous studies, especially modeling works. The key point of this paper is to show how this process is important for specific regions and different part of China from a perspective of long-term trend. It will be better that the authors give more descriptions on the aerosol-PBL feedback in the introduction part based on existing studies. In the introduction part, it also could be directly pointed out that the aerosol-PBL feedback will cause enhanced lower PBL pollution and decreased upper PBL pollution, as that showing in Fig.1b of Ding et al. (2016).**

Response: We have added the reference and the following description of the mechanism behind the aerosol-PBL feedback in the introduction.

Changes in manuscript: Page 2, line 18-27, text was added as: "Through scattering and absorption of solar radiation, atmospheric aerosols reduce net surface shortwave radiation (SSR) and thus induce surface cooling. The decreased net SSR reduces sensible heat fluxes (Zhang et al., 2008), which leads to weakened surface buoyancy fluxes (Tesfaye et al., 2014). Moreover, black carbon aerosols absorb solar radiation in the visible wavelengths and consequently warm up and stabilize the atmosphere. The changes in atmospheric radiative heating rate and atmospheric stability depend on the vertical distribution of aerosols (Gonçalves et al., 2015). If the absorbing aerosols are confined to the PBL, they may incur or strengthen a temperature inversion below the entrainment zone, leading to the suppression of vertical motions and to a shallower PBL (Barbaro et al., 2013). This creates unfavorable atmospheric conditions for pollution dispersion and thus worsens surface air pollution. This mechanism was demonstrated clearly in a recent modeling study by Ding et al. (2016). They showed that the aerosol-PBL feedback tends to increase lower PBL pollution and decrease upper PBL pollution."

Specific Comments 2: **A decrease of AOD at an altitude about 1km might also been influenced by cloud or mountain fog, in which the in-cloud removal/deposition could also cause a decreased upper altitude negative trend. How did the model deal with the cloud cover issue under high cloud cover condition? Did the authors exclude the days with thick cloud while categorizing days into relatively clean, moderate pollution, and severe pollution scenarios? It will be better to clarify these points in the paper.**

Response: As pointed out in the comments, the influence of cloud and mountain fog may result in an incorrect AOD trend at altitudes above 1000 m. The focus of our work is the aerosol trend and the aerosol-PBL feedback under clear-sky conditions, so the first step is to discriminate between clear and cloudy/foggy

conditions. The cloud screening procedures used are added to Section 2 of the revised manuscript.

Following the procedure, cloudy measurements were filtered out and the rest of the measurements were categorized according to pollution level: relatively clean, moderately polluted, and severely polluted. Atmospheric radiative heating rates under cloud-free conditions were then simulated.

Changes in manuscript: Page 3, line 26 – page 4, line 3, text was added as: "The focus of our work is on the trend in aerosols and the aerosol-PBL feedback under clear-sky conditions, so the first step is to discriminate between clear and cloudy/foggy conditions. A threshold of 90% in relative humidity (RH) is widely used to distinguish between haze (RH < 90%) and fog (RH > 90%) in visibility datasets (Chen and Wang, 2015). However, Ding and Liu (2014) suggested that a value of ~82% may be more suitable for differentiating between haze and fog over China. We use an intermediate value of 85% in our study. For AOD and aerosol extinction profile retrievals from the MFRSR and the MPL, the automated cloud identification algorithm proposed by Alexandrov et al. (2004) was used to screen out cloud-contaminated data. Cloud-free AOD retrievals from the MFRSR are subsequently used to constrain MPL-derived aerosol extinction coefficient profiles according to Welton et al. (2000). It is important to assure that there are no clouds along the pathway of the MPL laser beam when obtaining vertically-integrated aerosol extinction coefficients from the MPL. The column-integrated AOD from the MPL and the AOD retrieved from the MFRSR should be consistent."

Specific Comments 3: **The overall structure of the presentation could be a little bit changed. For example, Fig. 1-5 present results from Guangzhou Plain except Fig. 3, which shows results in the entire China (similar to Fig. 8), and was discussed in the second paragraph of Sec.3.1. How about discussing the Guanzhong Plain results in the first half of the main results part and the results for entire or different regions of China in the latter half? I think it**

will improve the readability. For Fig. 3 and Fig. 8, the region definition (i.e. range of longtidue and latitude) of data for the plot should be included.

Response: We appreciate your suggestions. Figure 2b and Fig. 3 in Section 3.1 are presented to show that the visibility trends seen in Fig. 2a are reliable and not the result of an artifact due to the influence of clouds or fog. Figure 3 is also referred to in Section 3.4 to confirm that the trend in the column-integrated AOD is much weaker than that of surface visibility. Figure 8 (**Renamed as Figure 9 in the revised manuscript**) is mainly used to show the distinct aerosol-PBL feedback induced by different light-absorbing properties of aerosols. Since the SSA in many parts of China is moderately low (~0.90), similar to the GZP, Figs. 2–7 are concerned with the main thrust of the study, namely aerosol-PBL interactions due to aerosol absorption. Therefore, we would like to keep the current structure of the paper.

The regions of study shown in Figs. 3 and 9 are given in Fig. S2 and Fig. S3, respectively.

Changes in manuscript: The term "The specific region of study can be found in Fig. S2" has been added in Fig. 3 caption. And, the term "The specific region of study can be found in Fig. S3" has been added in Fig. 9 caption.

Specific Comments 4: In terms of the calculation of heating rate, it highly depends on light-absorbing property of aerosols. Thus the SSA input data is vital, which ought to be provided in the main text. Additionally, the aerosol-boundary layer feedback play more important role in winter extreme pollution event. How about results during winter?

Response:

a) SSA values

SSA is indeed a key variable in determining the sign of the aerosol radiative forcing as well as the magnitude of the heating rate induced by aerosols. In our study, the values of SSA (i.e., 0.84 and 0.80 at 470 and 660 nm, respectively) are

taken directly from Lee et al. (2007). In addition, two years of visibility data from surface meteorological observations and BC concentrations measured by an aethalometer (Model AE-31) at the Xi'an site (108.97°E, 34.43°N) are used to evaluate the SSA reported by Lee et al. (2007). According to Xia et al. (2015), visibility measurements are converted to extinction coefficients (in km^{-1}) using the following relationship: 3.912/visibility. Absorption coefficients at 532 nm (in km^{-1}) are calculated as $(8.28\times M_{BC}+2.23)/1000$, where M_{BC} is the BC concentration measured by the AE-31 at 880 nm in units of $\mu g\cdot m^{-3}$ (Wu et al., 2009). Using the aforementioned aerosol absorption coefficients from the AE-31 and the aerosol extinction coefficients from visibility data, the corresponding SSA values at 532 nm over the GZP for the years 2011 and 2012 were calculated. The seasonal mean summertime SSA at Xi'an in 2011 and 2012 is 0.79 and 0.83, respectively. The values in winter are 0.76 and 0.77, respectively. The observation-based results in summer generally concur with those from the study of Lee et al. (2007).

b) Wintertime results

We have added Fig. 10 which shows the profile of AOD trends at different altitudes in winter in the revised manuscript (see page 23). As shown in the added figure, the profile of AOD trends at different altitudes in winter is similar to that in summer (Fig.3a). The major difference between the two is that the transition from negative to positive values in AOD trends takes place at a lower altitude. This is because the PBL height is generally lower in winter than in summer. Moreover, the transition zone in the long-term trends in surface visibility over the GZP shows a downward shift as well (not shown here). This finding attests to the notion that the aerosol-PBL feedback plays a more important role in winter.

However, unlike the results shown in Fig. 5a and 5b, the aerosol extinction coefficients above 1500 m during extreme pollution episodes in winter are larger than those during moderate pollution episodes based on MPL retrievals (Fig. R4). This is probably because the portion of AOD in the blind zone of the MPL (0–270 m) in winter is not negligible since pollution is constrained to a much shallower atmospheric layer in winter and cannot be properly removed from the

MFRSR-derived AOD, which is used to constrain the aerosol extinction coefficient profile. In other words, the portion of AOD in the lowest 270 m was artificially added to that above 270 m. The magnitude of that portion of AOD is highest during extreme pollution episodes in winter. As a result, the aerosol extinction coefficients are significantly overestimated at all altitudes during extreme pollution episodes.

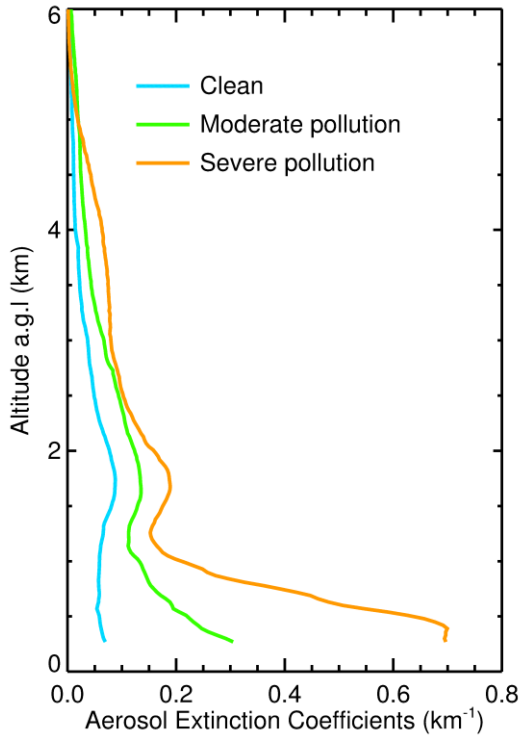

Fig. R4. Mean wintertime aerosol extinction profiles measured by the MPL in 2014 under different pollution level conditions. Profiles representing relatively clean, moderate pollution and severe pollution scenarios are shown as blue, green, and yellow lines, respectively. The "a.g.l" in the ordinate labels stands for "above ground level".

Changes in manuscript: The values of SSA were added in the text. Page 6, line 32, text was added as: **"**SSAs (i.e., 0.84 and 0.80 at 470 and 660 nm, respectively) taken from Lee et al. (2007)"

We have added Fig. 10 which shows the profile of AOD trends at different altitudes in winter and its corresponding descriptions in the revised manuscript.

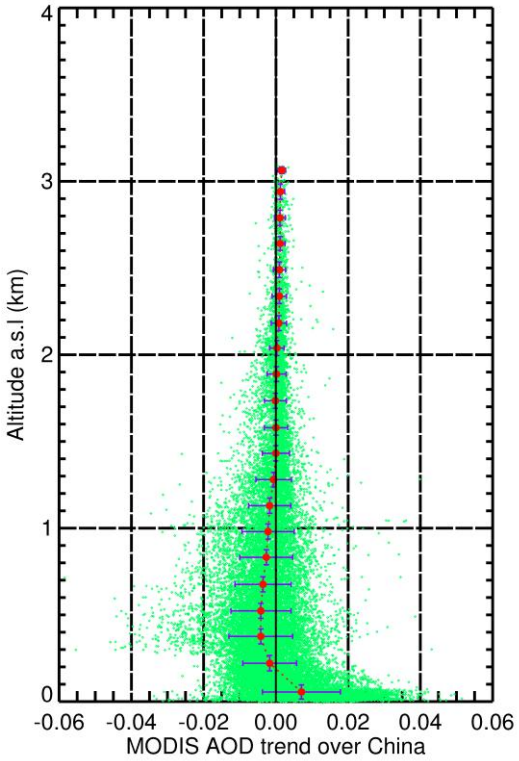

Fig. 10. Vertical profiles of the trend in aerosol optical depth (AOD) from MODIS-Aqua in the winter seasons of 2002 to 2014 over the entirety of China.The "a.s.l" in the ordinate labels stands for "above sea level".

Page 9, line 30 – page 10, line 3, text was added as: "Even though the MODIS AOD retrievals are relatively limited in winter due to the bright surface, the trend in AOD at different altitudes over the entirety of China are examined as well. As shown in Fig. 10, the profile of AOD trends at different altitudes in winter is similar to that in summer (Fig. 3a). The major difference between the two is that

the transition from negative to positive values in AOD trends takes place at a lower altitude. This is because the PBL height is generally lower in winter than in summer. Moreover, the transition zone in the long-term trends in surface visibility over the GZP show a downward shift as well (not shown here). This finding attests to that the aerosol-PBL feedback plays a more important role in winter."

Specific Comments 5: Both of MODIS and MISR retrievals display substantial upper-level decline in AOD trends. For the near-surface increasing AOD, MISR shows much smaller change. What are the causes for these differences?

Response: The smaller AOD trend values from MISR compared to MODIS at low altitudes can be mostly attributed to the difference in the spatial sampling and spatial resolution of the two instruments. Fig. 6 and its corresponding descriptions have been added in the text to further explain the causes for these differences.

Changes in manuscript: Page 4, line 22 – page 5, line 3, text was added as: "The difference in the spatial sampling and spatial resolution of the two instruments may explain why MISR AOD trend values are smaller than those from MODIS. As shown in Fig. 4 and Fig. 5a and 5b, the variation in AOD (or aerosol extinction coefficient) with altitude is more dramatic at low altitudes than at high altitudes. As a result, when AOD retrievals are averaged onto grids over undulating areas at different altitudes, the AOD, as well as the AOD trend, within the grid boxes at low altitudes will be smoothed out. To further investigate this, MODIS level 2 aerosol products were averaged onto 0.2°×0.2° latitude/longitude grids in the same manner as the MISR aerosol products. Comparisons between MODIS AOD trend profiles for different grid sizes (i.e., 0.1°×0.1° and 0.2°×0.2°) are shown in Fig. 6. There is almost no difference above 500 m. AOD trend values from the gridded data at the 0.2°×0.2° spatial resolution are much smaller than those at the 0.1°×0.1° spatial resolution, suggesting that the smoothing effect induced by a lower spatial resolution exists.

Although MODIS and MISR AOD data are averaged using the same grid size, AOD trend values from MODIS (blue dots in Fig. 6) at low altitudes are still larger than those from MISR (Fig. 3b). Zhang and Reid (2010) demonstrated that even if MODIS and MISR AOD retrievals were averaged onto the same 1°×1° latitude/longitude grid, MISR trends were still half that of the MODIS trends due to the spatial sampling differences of the two instruments."

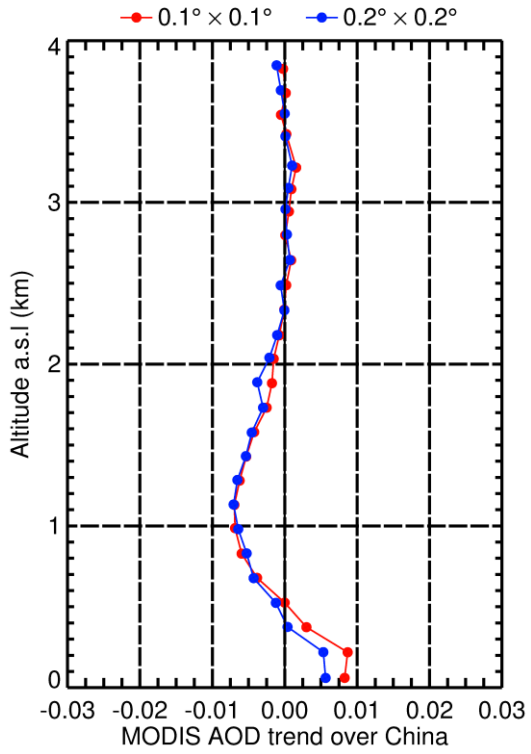

Fig. 6. Vertical profiles of aerosol optical depth (AOD) trends over the entirety of China from gridded MODIS AOD data at 0.1°×0.1° (red dots and red line) and 0.2°×0.2° (blue dots and blue line) spatial resolutions from 2002 to 2014.

References

Alexandrov, M. D., Marshak, A., Cairns, B., Lacis, A. A., and Carlson, B. E.: Automated cloud screening algorithm for MFRSR data, Geophys. Res. Lett., 31, L04118, doi:10.1029/2003GL019105, 2004.

Barbaro, E., Arellano, V. G., Krol, M. C., and Holtslag, A. A.: Impacts of aerosol shortwave radiation absorption on the dynamics of an idealized convective atmospheric boundary layer, Bound-Lay. Meteorol., 148(1), 31–49, doi:10.1007/s10546-013-9800-7, 2013.

Chen, H. P., and Wang, H. J.: Haze days in North China and the associated atmospheric circulations based on daily visibility data from 1960 to 2012, J. Geophys. Res. Atmos., 120, 5895–5909, doi:10.1002/2015jd023225, 2015.

Ding, A. J., Huang, X., Nie, W., Sun, J. N., Kerminen, V. M., Peteja, T., Su, H., Cheng, Y. F., Yang, X. Q., Wang, M. H., Chi, X. G., Wang, J. P., Virkkula A., Guo, W. D., Yuan, J., Wang, S. Y., Zhang, R. J., Wu, Y. F., Song, Y., Zhu, T., Zilitinkevich, S., Kulmala, M., and Fu, C. B.: Enhanced haze pollution by black carbon in megacities in China, Geophys. Res. Lett., 43, 2873–2879, doi:10.1002/2016gl067745, 2016.

Ding, Y. H., and Liu Y. J.: Analysis of long-term variations of fog and haze in China in recent 50 years and their relations with atmospheric humidity, Sci. China: Earth Sci., 57, 36–46, doi:10.1007/s11430-013-4792-1, 2014.

Gonçalves, W. A., Machado, L. A., and Kirstetter P. E.: Influence of biomass aerosol on precipitation over the Central Amazon: an observational study, Atmos. Chem. Phys., 15, 6789–6800, doi:10.5194/acp-15-6789-2015, 2015.

Lee, K. H., Li, Z., Wong, M. S., Xin, J. Y., Wang, Y. S., Hao, W. M., and Zhao, F. S.: Aerosol single scattering albedo estimated across China from a combination of

ground and satellite measurements, J. Geophys. Res. Atmos., 112, D22S15, doi:10.1029/2007jd009077, 2007.

Tesfaye, M., Botai, J., Sivakumar, V., and Tsidu, G. M.: Simulation of biomass burning aerosols mass distributions and their direct and semi-direct effects over South Africa using a regional climate model, Meteorol. Atmos. Phys., 125(3), 177–195, doi:10.1007/s00703-014-0328-2, 2014.

Welton, E. J., Voss, K. J., Gordon, H. R., Maring, H., Smirnov, A., Holben, B., Schmid, B., Livingston, J. M., Russell, P. B., Durkee, P. A., Formenti, P., and Andreae, M. O.: Ground-based lidar measurements of aerosols during ACE-2:instrument description, results, and comparisons with other ground-based and airborne measurements, Tellus, 52, 636–651, doi: 10.1034/j.1600-0889.2000.00025.x, 2000.

Wu, D., Mao, J. T., Deng, X. J., Tie, X. X., Zhang. Y. H., Zeng, L. M., Li, F., Tan, H. B., Bi, X. Y., Huang, X. Y., Chen, J. and Deng T.: Black carbon aerosols and their radiative properties in the Pearl River Delta region, Sci. China - Earth Sci., 52(8), 1152–1163, doi:10.1007/s11430-009-0115-y, 2009.

Xia, H. Y., Shentu, G., Shangguan, M. J., Xia, X. X., Jia, X. D., Wang, C., Zhang, J., Pelc, J. S., Fejer, M. M., Zhang, Q., Dou, X. K., and Pan J. W.: Long-range micro-pulse aerosol lidar at 1.5 μm with an upconversion single-photon detector, Opt. Lett., 40(7), 1579–1582, doi:10.1364/OL.40.001579, 2015.

Zhang, J., and Reid, J. S.: A decadal regional and global trend analysis of the aerosol optical depth using a data-assimilation grade over-water MODIS and Level 2 MISR aerosol products, Atmos. Chem. Phys., 10, 10949–10963, doi:10.5194/acp-10-10949-2010, 2010.

Zhang, Y., Fu, R., Yu, H. B., Dickinson, R. E., Juarez, R. N., Chin, M., and Wang, H.: A regional climate model study of how biomass burning aerosol impacts land-atmosphere interactions over the Amazon, J. Geophys. Res. Atmos., 113,d14s15, doi:10.1029/2007jd009449, 2008.

Opposite Long-term Trends in Aerosols between Lower and Higher Altitudes: A Testimony to the Aerosol-PBL Feedback

Zipeng Dong[1,2], Zhanqing Li[1,3], Xing Yu[2], Maureen Cribb[3], Xingmin Li[2], and Jin Dai[2]

[1]College of Global Change and Earth System Science, Beijing Normal University, Beijing, 100875, China
[2]Meteorological Institute of Shaanxi Province, Xi'an, 710014, China
[3]Department of Atmospheric and Oceanic Science, University of Maryland, College Park, MD 20742, USA

Correspondence to: Zhanqing Li (zli@atmos.umd.edu)

Abstract. Interactions between absorbing aerosols and the planetary boundary layer (PBL) play an important role in enhancing air pollution near the surface. In this study, a unique feature of the interaction is found that has important implications in monitoring and combating air pollution. Opposite trends in aerosol loading between the lower and upper PBL are found on a wide range of time scales and from different types of data acquired by various platforms: from a short-term field experiment to decadal satellite observations, and multi-decadal ground observations in China. A novel method is proposed to obtain the vertical profiles of aerosol loading from passive sensors by virtue of varying elevations. Trend analyses of three particulate variables having different temporal scales, namely, visibility, aerosol optical depth, and extinction, all exhibit the same trend: increasing ~~at~~ in the lower atmosphere, but decreasing in the upper atmosphere. Column-integrated quantities are much less variable. The reversal trend is consistent with the strong vertical gradients in the aerosol-induced atmospheric heating rate that unevenly modifies the atmospheric temperature profile and alters the stability differently. These findings have multiple implications in understanding and combating air pollution, especially in many developing countries producing large amounts of black and brown carbon aerosols.

1 Introduction

Air pollution induced by rapid industrialization and urbanization over the past decades has become a critical constraint for sustainable development in China. Particulate pollutants, or aerosols in general, can also alter weather and climate due to their radiative and microphysical effects. Heavy aerosol loading over China as revealed by both ground and satellite observations has a significant influence on a wide range of meteorological variables and may play significant roles in the climate change of China (Wu et al., 2016) and the Asian monsoon system (Li et al., 2016).

The frequent occurrence of hazy weather in China has severely undermined people's lives. Average concentrations of particulate matter (PM) with aerodynamic diameters < 10 μm (PM10) and < 2.5 μm (PM2.5) at urban/suburban sites in China from 2006 to 2014 are 83.6 and 56.3 μg m^{-3}, respectively, while values at rural stations are 54.8 and 30.8 μg m^{-3},

respectively (Y. Wang et al., 2015). Mean ground-level PM2.5 concentrations observed over the North China Plain and the Guan-Zhong Plain (GZP) exceed the latest air quality standards of China by about several times (Y. Wang et al., 2015). Long-term exposure to ambient PM may have led to significant increases in cardiorespiratory mortality in China (Chen et al., 2013; Yin et al., 2015). The mean aerosol optical depth (AOD) observed by sun photometers in rural and urban sites over China was 0.34 and 0.74, respectively (Lee et al., 2007; Che et al., 2015), which is well above the global average of 0.17 (Lee and Chung, 2013).

Economic development plays an important role in dictating air quality in China. The spatial and temporal distributions of AOD and PM2.5 are also affected by urbanization and topography (Li and Wang, 2014). Through the study of extreme air pollution events, the interaction between absorbing aerosols and the planetary boundary layer (PBL) height (PBLH) was recognized as an important contributor to the accumulation of PM in the near-surface atmosphere over China (Wendisch et al., 2008; Ding et al., 2013). Together with fossil fuel combustion, biomass burning is the main source releasing absorbing aerosols into the atmosphere. Besides the urban/industrial pollution, Zhang et al. (2008) and Tesfaye et al. (2014) demonstrated that the biomass burning aerosols have an important impact on the evolution of PBL as well. A broad theoretical perspective of the impact of absorbing aerosols on the PBL was hypothesized by Wang et al. (2013), suggesting that a feedback between the PBLH and absorbing aerosols may play a key role in the aggravation of surface pollution during heavy pollution episodes. Through scattering and absorption of solar radiation, atmospheric aerosols reduce net surface shortwave radiation (SSR) and thus induce surface cooling. The decreased net SSR reduces sensible heat fluxes (Zhang et al., 2008), which leads to weakened surface buoyancy fluxes (Tesfaye et al., 2014). Moreover, black carbon aerosols absorb solar radiation in the visible wavelengths and consequently warm up and stabilize the atmosphere. The changes in atmospheric radiative heating rate and atmospheric stability depend on the vertical distribution of aerosols (Gonçalves et al., 2015). If the absorbing aerosols are confined to the PBL, they may incur or strengthen a temperature inversion below the entrainment zone, leading to the suppression of vertical motion and to a shallower PBL (Barbaro et al., 2013). This creates unfavorable atmospheric conditions for pollution dispersion and thus worsens surface air pollution. This mechanism was demonstrated clearly in a recent modelling study by Ding et al. (2016). They showed that the aerosol-PBL feedback tends to increase lower PBL pollution and decrease upper PBL pollution.

In this study, we strive to obtain unique observational evidence that the aerosol-PBL feedback plays a special role in the long-term trend in air pollution, especially at the ground level, using both ground-based and historical satellite measurements.

2 Data

We used three types of measurements: long-term surface visibility measurements, medium-term satellite retrievals, and short-term field experiment measurements to take advantage of the merits of each product.

Visibility data obtained by China Meteorological Administration (CMA) stations located on the GZP are used here as a proxy for air quality at the surface, while AOD retrieved from the Moderate Resolution Imaging Spectroradiometer (MODIS) and the Multi-angle Imaging Spectro-Radiometer (MISR) are used to denote total aerosol loading in the atmospheric column. Operational MODIS level 2 aerosol products with a spatial resolution of 10 km at nadir and MISR level 2 aerosol products with a spatial resolution of 17.6 km were used to generate gridded AOD data at every 0.1°×0.1° latitude/longitude pair and 0.2°×0.2° latitude/longitude pair over China, respectively.

The GZP is a key economic zone in western-central China, located along the lower valley of the Wei River (Fig. 1a). As one of the most densely populated regions of China, the GZP covers an area of 34000 km^2 and has a population of about 25 million people. The average altitude of the plain is around 500 meters. Xi'an is the largest and most developed city in the plain. As shown in Fig. 1, the spatial distribution of AOD follows the topography closely, i.e., higher over the basin than over the surrounding hilly mountain area.

The Qinling Atmospheric Environment Observation Experiment was conducted at the Changan meteorological station in the southern suburb of Xi'an (34.150°N, 108.917°E, 433 m above sea level) and at the nearby Qinling Mountains. Measurements of aerosols and atmospheric radiation have been made since May 2013 at Changan. Its goal is to investigate the impact of heavy aerosol loading on radiation, clouds, and climate in central China. A multi-filter rotating shadowband radiometer (MFRSR) and a set of broadband radiometers were operated side by side. A micro-pulse lidar (MPL) manufactured by the Sigma Space Corporation was used to obtain aerosol profiles. Based on solar radiation measurements from the MFRSR, the Langley technique was used to retrieve AODs in the visible and near-infrared spectral bands.

The focus of our work is on the trend in aerosols and the aerosol-PBL feedback under clear-sky conditions, so the first step is to discriminate between clear and cloudy/foggy conditions. A threshold of 90% in relative humidity (RH) is widely used to distinguish between haze (RH < 90%) and fog (RH > 90%) in visibility datasets (Chen and Wang, 2015). However, Ding and Liu (2014) suggested that a value of ~82% may be more suitable for differentiating between haze and fog over China. We use an intermediate value of 85% in our study. For AOD and aerosol extinction profile retrievals from the MFRSR and the MPL, the automated cloud identification algorithm proposed by Alexandrov et al. (2004) was used to screen out cloud-contaminated data. Cloud-free AOD retrievals from the MFRSR are subsequently used to constrain MPL-derived aerosol

extinction coefficient profiles according to Welton et al. (2000). It is important to assure that there are no clouds along the pathway of the MPL laser beam when obtaining vertically-integrated aerosol extinction coefficients from the MPL. The column-integrated AOD from the MPL and the AOD retrieved from the MFRSR should be consistent.

3 Trend analyses

3.1 Trends in visibility and AOD

The very rapid urbanization and economic development in China from the 1980s until the present has resulted in serious pollution problems in this region, as shown by the trend in visibility measurements made at stations located at altitudes less than 1 km (Fig. 2a). Note that the two are anti-correlated: poor visibility corresponds to high AOD (Fig. 2b). From 1980 to about 2008, visibility over the lowland of the GZP had been declining. A turnaround has occurred since then with a more dramatic improvement in visibility occurring over the past few years when Chinese central and local governments began to take action toward curbing air pollution. This increase in visibility was accompanied by a decrease in AOD, which is seen in both ground and satellite observations. However, a different trend in visibility measured at the high mountain stations (altitudes over 1 km) is seen, i.e., a general increasing trend since 1980, suggesting that air quality over the mountains has been improving.

Note that visibility is often influenced by local emissions and fog whose long-term trends may contribute to visibility trends. To overcome this limitation, we also analyzed trends in AOD clustered according to topography so that each set of AODs represents the aerosol loading at some level above ground. By varying the ground elevation, we can derive profiles of AOD trends at different altitudes as shown in Fig. 3 using both MODIS and MISR data. AOD retrievals from both satellite products show that the trend in AOD varies with height, i.e., increasing at low altitudes but decreasing at higher altitudes. We hypothesize that this switch in trend with height results from the feedback between absorbing aerosols and the PBLH. The difference in the spatial sampling and spatial resolution of the two instruments may explain why MISR AOD trend values are smaller than those from MODIS. As shown in Fig. 4 and Fig. 5a and 5b, the variation in AOD (or aerosol extinction coefficient) with altitude is more dramatic at low altitudes than at high altitudes. As a result, when AOD retrievals are averaged onto grids over undulating areas at different altitudes, the AOD, as well as the AOD trend, within the grid boxes at low altitudes will be smoothed out. To further investigate this, MODIS level 2 aerosol products were averaged onto 0.2°×0.2° latitude/longitude grids in the same manner as the MISR aerosol products. Comparisons between MODIS AOD trend profiles for different grid sizes (i.e., 0.1°×0.1° and 0.2°×0.2°) are shown in Fig. 6. There is almost no difference above 500 m. AOD trend values from the gridded data at the 0.2°×0.2° spatial resolution are much smaller than those at the 0.1°×0.1° spatial resolution, suggesting that the smoothing effect induced by a lower spatial resolution exists. Although MODIS and MISR AOD data are averaged using the same grid size, AOD trend values from MODIS (blue dots in Fig. 6) at

low altitudes are still larger than those from MISR (Fig. 3b). Zhang and Reid (2010) demonstrated that even if MODIS and MISR AOD retrievals were averaged onto the same 1°×1° latitude/longitude grid, MISR trends were still half that of the MODIS trends due to the spatial sampling differences of the two instruments.

3. 2 Variation of the trend with height

The proportion of light-scattering aerosol components, e.g., nitrate and sulphate, to the total PM2.5 in Xi'an is much lower than that in other big cities such as Beijing, Shanghai, and Guangzhou, while the proportion of light-absorbing aerosol components, e.g., black carbon and dust, is much higher (Huang et al., 2014). The single scattering albedo (SSA) over this region is well below 0.85, while the mean SSA in China is ~0.9 and high in southeast China, as derived by Lee et al. (2007) from a combination of satellite and ground observations across China. Absorbing aerosols trap solar radiation in the atmosphere with much more intensive heating in the upper PBL than in the lower atmosphere. This could lead to a significant decrease in the PBLH, which tends to increase near-surface particulate concentrations.

However, the aforementioned process is complex and difficult to evaluate by direct observations due to the influence of other factors, such as the large-scale circulation, local pollutant emissions, and atmospheric transport. Therefore, the study of the interaction between aerosols and the PBLH has thus far been mainly achieved through model simulations or by studying short-term extreme pollution cases. The complex terrain of the GZP hinders the advective diffusion of pollution (Zhao et al., 2015a) and thus provides a unique opportunity to study the interaction between aerosols and the PBLH. Here we attempt to illustrate the impact of aerosols on the evolution of the PBL and the feedback between them by using long-term observations from the GZP.

3.3 Comparison of profiles of aerosol extinction from satellite and lidar

Profiles of aerosol extinction were derived from MPL backscattering measurements in conjunction with MFRSR AOD data following the method of Welton et al. (2000). Data collected at the Changan station during the summers of 2013 and 2014 were used in this study to characterize the aerosol vertical distribution.

Due to a lack of long-term MPL observations, we propose a novel approach of obtaining profiles of aerosol extinction from AOD measurements at different altitudes by assuming that aerosols are homogeneously distributed across the basin surrounded by the Qinling Mountains and the Loess Plateau. Data from the summers of 2002-2014 extracted from the Collection 6 MODIS-Aqua AOD product is used. Unlike other plains, the GZP is rarely influenced by large-scale circulations because airflow is blocked by the 1500-km long Qinling mountain range. Also, the regional prevailing winds over the GZP are unfavorable for the horizontal transport of PM (Zhao et al., 2015b). As a result, particles are mostly confined to their source region and tend to accumulate in the lowlands (Zhao et al., 2015a). In this case, aerosols may be

well-mixed over the valley. The AOD at a given location and at an elevation of z (in m), denoted as AOD_z, is defined as the integrated extinction coefficient over the vertical path from the surface to the top of atmosphere (TOA):

$$AOD_z = \int_z^{TOA} \beta_{z'} dz' \qquad (1)$$

where $\beta_{Z'}$ is the extinction coefficient at a height of z'.

If the hypothesis is true, the observed AODs at the same elevation over the GZP should be similar. To test this, comparisons were made between the MODIS AOD at different altitudes and the integrated extinction coefficient obtained from the MPL. As shown in Fig. 4, the AOD at different altitudes (green dots) and MPL data (black dots) are generally consistent. Note that the MPL detects vertical profiles of aerosols directly above the observation site in the GZP, while MODIS AOD retrievals are spatially distributed over the rugged terrain surrounding the plain. The distance between MODIS AOD pixels at varying altitudes and the MPL site at the Changan station increases with altitude. Consequently, profiles derived from MODIS AOD at different locations having different altitudes represent basin-wide (including the perimeters of the surrounding mountains) profiles. Profiles from the MPL were obtained at a fixed site. As such, the agreement between the AODs at varying altitudes from the MPL and MODIS attests to the validity of our assumption that the vertical mixing is uniform across the basin.

Thus, AOD with respect to any vertical path segment going from z0 to z1, denoted as $AOD_{z0\text{-}z1}$, can be computed by integrating the extinction coefficient β_Z' over the corresponding altitude range or by subtracting the AOD observed at z0 from that observed at z1:

$$AOD_{z0-z1} = \int_{z0}^{z1} \beta_{z'} dz' = \int_{z0}^{TOA} \beta_{z'} dz' - \int_{z1}^{TOA} \beta_{z'} dz' = AOD_{z0} - AOD_{z1} \qquad (2)$$

In this way, any portion of AOD at a given altitude range can be obtained from a combination of MODIS AOD data and Advanced Spaceborne Thermal Emission and Reflection Radiometer (ASTER) global digital elevation model (GDEM) standard data products at a 30-m spatial resolution (http://reverb.echo.nasa.gov/reverb). Gridded mean summertime AODs for the period 2002–2014 are first created by gridding the high-quality (q~~Q~~uality a~~A~~ssurance c~~C~~onfidence f~~F~~lag = 3) granule-level MODIS AOD retrievals onto a daily 0.1°-longitude × 0. 1°-latitude grid ~~for the period 2002–2014~~. The mean AOD is then calculated by ~~taking the average of~~ averaging the daily AODs in each grid box. Grid boxes over the GZP ~~having~~ containing elevations from the GDEM with high relative standard deviations (> 10%) are not included in the analysis because the AOD in those boxes can vary considerably due to the elevation inhomogeneity.

To illustrate the impact of aerosols on the vertical temperature structure, the Santa Barbara DISORT Atmospheric Radiative Transfer (SBDART) model (Ricchiazzi et al., 1998) was used in this study to simulate the atmospheric heating rate induced by absorbing aerosols. The aerosol inputs to the SBDART model are AODs, Ångström exponents retrieved from MFRSR measurements, SSAs (i.e., 0.84 and 0.80 at 470 and 660 nm, respectively) taken from Lee et al. (2007), and aerosol

extinction profiles at 532 nm obtained from the MPL. The mid-latitude summer atmospheric profile adopted in the SBDART model was used in simulations. Additional input parameters include MODIS surface reflectance (http://ladsweb.nascom.nasa.gov/data/search.html), ozone column amounts from the Ozone Monitoring Instrument (https://ozoneaq.gsfc.nasa.gov/data/ozone/), and precipitable water vapor from the MFRSR.

3.4 Coupling between the PBL and aerosol absorption

The aerosol extinction profiles obtained from co-located MFRSR and MPL measurements were classified into three categories based on the quartiles of the aerosol loading in the lowest 270–870 m of the atmosphere:

1) clean condition: in the first quartile,
2) moderate pollution: between the second and third quartile,
3) severe pollution: the fourth quartile.

An altitude of 270 m was chosen as the lower limit because of missing data in the blind zone of the MPL (0–270 m). The upper limit of 870 m is a value established by Song et al. (2013) who found that ~50% of aerosols were confined to the lowest 600 m of the atmosphere over Lanzhou, a city surrounded by mountains.

Aerosol profiles corresponding to the three pollution levels in the summers of 2013 and 2014 are shown in Fig. 5a and 5b. The column-integrated AODs for the clean, moderate pollution, and severe pollution categories are 0.23, 0.38, and 0.50 in Fig. 5a, respectively, and 0.24, 0.33, and 0.41 in Fig. 5b, respectively. The PBLH for the clean, moderate, and severe pollution cases in the summer of 2013 are 2.9, 2.4, and 1.2 km, respectively, and 2.2, 2.0, and 0.8 km, respectively, in the summer of 2014. As shown in Fig. 5a and 5b, the shapes of the aerosol profiles under each pollution condition in both years are similar ~~for all three pollution conditions~~, suggesting that these profiles are characteristic of the region. The relative changes in the level of pollution in the lower and upper PBL are generally out of phase. For the case of severe pollution (orange curve), pollution decreases most dramatically at the top of a presumably shallow PBL, whereas extinction increases with height for the clean and moderate pollution cases. Extinction coefficients above 1500 m for the severe pollution case are smaller than those in the moderate pollution case. Our finding suggests that a strong correlation exists between absorbing aerosols and the PBL over the GZP. However, causality cannot be established by such an analysis because the PBL strongly affects aerosols and vice versa.

Several simulation studies have demonstrated the coupling between absorbing aerosols and the PBL in China. Absorbing aerosols heat up the lower atmosphere due to aerosol absorption of solar radiation and cool down the lower PBL by reducing the amount of solar radiation reaching the earth's surface (Wendisch et al., 2008; Ding et al., 2013). Ding et al. (2016) found

that the PM2.5 mass concentration was significantly underestimated near the surface and overestimated around the top of the PBL when the impact of absorbing aerosols was neglected. Aerosols trapped in the basin increase atmospheric stability and suppress convection locally (Fan et al., 2015).

The parameterization schemes developed by Xia et al. (2007) were used to quantitatively estimate the aerosol-induced changes in the net SSR, namely the aerosol direct radiative forcing (ADRF) at the surface, at Xi'an by using the AOD retrievals from the MFRSR, the MODIS surface albedo products (MCD43B3), and the global shortwave radiation (SWR) measured by Kipp-Zonen CMP21 from June 2013 to August 2014. The diurnal variation of the ADRF in summer at Xi'an is shown in Fig. S1. The mean diurnal ADRF is -35.7 W m^{-2} for the global SWR at the surface in summer. And, the ADRF during the daytime showed very large negative values, indicating weakened surface buoyancy fluxes and decreased PBLH (Zhang et al., 2008; Tesfaye et al., 2014).

Aerosol heating rates computed during the course of the day (0800–1800 Beijing Time) in the summer are shown in Fig. 5c and 5d. The maximum heating rate occurs at ~1 km. In the relatively clean and moderate pollution scenarios, maximum heating rates are seen at higher altitudes. This suggests that the stability inside the PBL was strengthened while the instability above the PBL was enhanced, causing a "heat pump" effect (Lau and Kim, 2006) that favors the vertical diffusion of aerosol particles in the upper atmosphere. As a result, aerosol extinction coefficients observed at altitudes above 1500 m in the most polluted scenario are lower than in the moderately polluted scenario.

The visibility at ground level has significantly decreased in northern China from 2000 to 2012 (Chen and Wang, 2015) and the number of hazy days has increased noticeably (H. Wang et al., 2015). However, the column-integrated AOD has shown a much weaker trend as shown in Fig. 3 and in Lin et al. (2013). The disproportionate changes in surface visibility and column aerosol loading could be due to the rapid accumulation of particles near the surface in combination with a reduction in aerosol particles in the upper PBL due to the inefficient vertical transport of aerosol particles.

To test this conjecture, we used the MODIS AOD product to derive aerosol loading in the lower PBL (400-800 m, $AOD_{400\text{-}800m}$) and the upper PBL (1500-1900 m, $AOD_{1500\text{-}1900m}$) using the aforementioned method for each summer from 2002 to 2014. The aerosol scale height was calculated using an exponential curve fitting of MODIS AOD and ASTER GDEM data (Dong et al., 2013). The aerosol scale height is used as a proxy of the PBLH because it is related to the height of the boundary layer (Gerasopoulos et al., 2003). The scatterplots of $AOD_{400\text{-}800m}$ and $AOD_{1500\text{-}1900m}$ as a function of aerosol scale height in Fig. 7~~6~~ shows the difference in the response of the aerosol loading at different altitudes to the scale height. As the AOD near the surface increases from 0.2 to 0.6, the aerosol scale height drops from ~1100 m to 670 m. In response to the decrease in scale height, the aerosol loading above the PBL decreases. The correlation coefficients of the linear relationships

between $AOD_{400\text{-}800m}$ and $AOD_{1500\text{-}1900m}$, and the aerosol scale height are 0.71 and 0.55, respectively. The correlations are statistically significant at the 95% confidence level. However, the correlation coefficient of the linear relationship between $AOD_{1500\text{-}1900m}$ and $AOD_{400\text{-}800m}$ does not reach the 0.05 significance level, suggesting that the amount of aerosol particles near the surface has an indirect impact on the aerosol concentration in the upper PBL through its effect on the PBLH.

During the period of MODIS observations, the trend in AOD over China has a turning point around 2008: an upward trend pre-2008 followed by a downward trend post-2008, as reported by He et al. (2016). We examined the summertime trends in AOD at different altitudes during the period 2002–2008 (red line in Fig. 8~~7~~a) and 2008–2014 (blue line in Fig. 8~~7~~a). AOD over the lowlands (< 800 m) increased dramatically during the period 2002–2008. However, the AOD at higher altitudes (1.7–2.3 km) decreased at a rate of -0.0075 per year. It is worth emphasizing that the magnitude of this negative AOD tendency at high altitudes exceeds that of the ascending tendency over the entirety of China (+0.0003) during the same period (He et al., 2016), suggesting that the changes in AOD at higher altitudes over the GZP are different from the changes in other regions. For the period 2008–2014, the trends in AOD at different altitudes are opposite to those from the 2002–2008 period. The AOD over the lowlands with altitudes < 700 m dramatically decreased while AOD at altitudes from 800 to 1200 m increased. To further illustrate this phenomenon, the variation in aerosol extinction coefficient derived from d(AOD)/dz using MODIS AOD retrievals in conjunction with the GDEM is shown in Fig. 8~~7~~b. Concurrent with the increase in aerosol concentration in the lower PBL during the period 2002–2008, aerosol extinction coefficients at altitudes above 1850 m decreased with a maximum value occurring near 2300 m. The opposite is seen during the period 2008–2014. A notable downward tendency in the aerosol extinction coefficient in the lower PBL is found, while at the same time, a positive trend with a maximum magnitude of 0.04 km^{-1} yr^{-1} is seen at altitudes between 900 and 1300 m. The vertical distribution of trends in AOD and aerosol extinction coefficient during the two periods show that changes in aerosol loading near the surface were opposite to those above the PBLH over the GZP, which is solid evidence that the aerosol-PBL feedback plays a significant role in the long-term trend in air pollution, and especially in the opposite trends between the lower and upper PBL.

To further investigate the role of aerosol absorption in the opposite trends, we expanded our satellite analyses to over large areas in China containing aerosols with a different light-absorbing property. The SSA in northern China is generally lower than in southern China (Lee et al., 2007). It was thus hypothesized that the reversal trends in northern China would be more significant than in southern China, which is confirmed from the trend analyses at different altitudes over the entire period of MODIS observations shown in Fig. 9~~8~~.

Even though the MODIS AOD retrievals are relatively limited in winter due to the bright surface, the trend in AOD at different altitudes over the entirety of China are examined as well. As shown in Fig. 10, the profile of AOD trends at different altitudes in winter is similar to that in summer (Fig. 3a). The major difference between the two is that the transition

from negative to positive values in AOD trends takes place at a lower altitude. This is because the PBL height is generally lower in winter than in summer. Moreover, the transition zone in the long-term trends in surface visibility over the GZP show a downward shift as well (not shown here). This finding attests to that the aerosol-PBL feedback plays a more important role in winter.

4 Summary and conclusions

While an aerosol and PBL interaction has been conjectured, chiefly based on an inverse correlation between air pollution (both gas and particulate pollutants) and PBL height. This may not be construed as an evidence of the interaction because they may co-vary with meteorological conditions. A low PBL is favorable for the accumulation of any pollutant, but this does not imply that they interact with each other. For aerosols to interact with the PBL, the atmospheric thermodynamic status must be modified.

To obtain more direct evidence and to gain further insight into the interaction on both air pollution and PBL dynamics, we took advantage of rich measurements made from an intensive field experiment, long-term routine surface visibility observations, and satellite-based aerosol retrievals. A unique region in central China was chosen: the GZP and the Qinling mountain range composed of mountains having a wide range of heights. The GZP is one of the most heavily polluted regions in China due to coal-burning industries and has the lowest aerosol SSA measured in China. Next to the GZP lies the Qinling mountain range, which offers an opportunity to examine vertical profiles of aerosol loading through a novel method proposed here.

Using both the inferred and observed profiles of aerosol extinction together with computations of aerosol-induced radiative heating, a unique "signature" of the interaction between absorbing aerosols and the PBL is discovered, namely, the opposite trends in aerosol extinction, visibility, and aerosol optical depth as measured in the lower and upper PBL. Visibility data collected at meteorological stations located at altitudes below and above 1 km showed generally downward and upward trends, respectively, since 1980. The same opposite trends are also seen from retrievals of AOD from both MODIS and MISR since ~2000 over regions with altitudes below and above 1 km. Two years of lidar measurements showed that the vertical structure of the aerosol extinction coefficient varied systematically with the aerosol concentration in the lower atmosphere, i.e., a cleaner atmosphere near the surface corresponded to a higher peak in aerosol extinction and vice versa. As near-surface pollutants accumulate, they are confined to the lower PBL due to enhanced atmospheric stability, whereas pollutants in the upper PBL are dispersed more efficiently as the atmosphere becomes more unstable, thanks to heating in the lower PBL.

To further verify if it indeed stems from aerosol-PBL interactions, similar analyses were done in regions with distinctly different values of SSA. In low SSA regions, the reversal trends are much more pronounced than in high SSA regions, which attests to the critical role of aerosol absorption.

The findings presented in this study have numerous important implications. First, it signifies the importance of aerosol-PBL interactions in dictating ground-level pollution. In particular, it implies that particulate pollution at the ground level can be much heavier than what is denoted by a column-integrated AOD. The latter is relatively readily and widely available and has been used as a proxy for indices representing air pollution on the ground such as PM2.5 and PM10. In regions/periods dominated by absorbing aerosols, changes in AOD may be totally decoupled from ground-level PM concentrations. Second, it suggests that one may not be able to use ground-based measurements of pollutants to assess the effect of any emission controls. Taking China as an example, drastic measures have been taken to reduce emissions but they seem to have little impact on heavy haze episodes because a significant part of the real reduction may have occurred in the upper PBL at the expense of worsening air quality at the surface or lower atmosphere. Finally, it points to a more efficient means of reducing air pollution: reducing/removing absorbing aerosols such as soot or black carbon, which can cause far more serious pollution than non-absorbing aerosols such as sulfates.

Data availability

The ASTER GDEM and MODIS AOD data are available from http://reverb.echo.nasa.gov/reverb and https://ladsweb.nascom.nasa.gov/, respectively. The MPL-derived aerosol profiles and other relevant data are available upon request (contact: Zipeng Dong, dzp2003@126.com).

Acknowledgements

This work was supported by the National Natural Science Foundation of China (41675141, 41375155), the National Basic Research Program (973 Program) of China (2013CB955804), and the Joint National Natural Science Foundation of China - Israel Science Foundation Research Program (41561144004). We thank NASA for providing ASTER GDEM and MODIS AOD data.

References

Alexandrov, M. D., Marshak, A., Cairns, B., Lacis, A. A., and Carlson, B. E.: Automated cloud screening algorithm for MFRSR data, Geophys. Res. Lett., 31, L04118, doi:10.1029/2003GL019105, 2004.

Barbaro, E., Arellano, V. G., Krol, M. C., and Holtslag, A. A.: Impacts of aerosol shortwave radiation absorption on the dynamics of an idealized convective atmospheric boundary layer, Bound-Lay. Meteorol., 148(1), 31–-49, doi:10.1007/s10546-013-9800-7, 2013.

Che, H., Zhang, X. Y., Xia, X., Goloub, P., Holben, B., Zhao, H., Wang, Y., Zhang, X. C., Wang, H., Blarel, L., Damiri, B., Zhang R., Deng, X., Ma, Y., Wang, T., Geng F., Qi, B., Zhu, J., Yu, J., Chen, Q., and Shi, G.: Ground-based aerosol climatology of China: aerosol optical depths from the China Aerosol Remote Sensing Network (CARSNET) 2002–2013, Atmos. Chem. Phys., 15, 7619–7652, doi:10.5194/acp-15-7619-2015, 2015.

Chen, H. and Wang, H.: Haze days in North China and the associated atmospheric circulations based on daily visibility data from 1960 to 2012, J. Geophys. Res. -Atmos., 120, 5895–5909, doi: 10.1002/2015jd023225, 2015.

Chen, Y., Ebenstein, A., Greenstone, M., and Li, H. B.: Evidence on the impact of sustained exposure to air pollution on life expectancy from China's Huai River policy, P. Natl. Acad. Sci. USA, 110, 12936–12941, doi:10.1073/pnas.1300018110, 2013.

Ding, A. J., Fu, C. B., Yang, X. Q., Sun, J. N., Peteja, T., Kerminen, V. M., Wang, T., Xie, Y. N., Herrmann, E., Zheng, L. F., Nie, W., Liu, Q., Wei, X. L., and Kulmala, M.: Intense atmospheric pollution modifies weather: a case of mixed biomass burning with fossil fuel combustion pollution in eastern China, Atmos. Chem. Phys., 13, 10545–10554, doi:10.5194/acp-13-10545-2013, 2013.

Ding, A. J., Huang, X., Nie, W., Sun, J. N., Kerminen, V. M., Peteja, T., Su, H., Cheng, Y. F., Yang, X. Q., Wang, M. H., Chi, X. G., Wang, J. P., Virkkula A., Guo, W. D., Yuan, J., Wang, S. Y., Zhang, R. J., Wu, Y. F., Song, Y., Zhu, T., Zilitinkevich, S., Kulmala, M., and Fu, C. B.: Enhanced haze pollution by black carbon in megacities in China, Geophys. Res. Lett., 43, 2873–2879, doi: 10.1002/2016gl067745, 2016.

Ding, Y. H. and Liu Y. J.: Analysis of long-term variations of fog and haze in China in recent 50 years and their relations with atmospheric humidity, Sci. China: Earth Sci., 57, 36–46, doi: 10.1007/s11430-013-4792-1, 2014.

Dong, Z. P., Yu, X., Li, X. M., and Dai, J.: Analysis of variation trends and causes of aerosol optical depth in Shaanxi Province using MODIS data, Chinese Sci. Bull., 58, 4486–4496, doi:10.1007/s11434-013-5991-z, 2013.

Fan, J. W., Rosenfeld, D., Yang, Y., Zhao, C., Leung, L. R., and Li, Z. Q.: Substantial contribution of anthropogenic air pollution to catastrophic floods in Southwest China, Geophys. Res. Lett., 42, 6066–6075, doi:10.1002/2015gl064479, 2015.

Gerasopoulos, E., Andreae, M. O., Zerefos, C. S., Andreae, T. W., Balis, D., Formenti, P., Merlet, P., Amiridis, V., and Papastefanou, C.: Climatological aspects of aerosol optical properties in Northern Greece, Atmos. Chem. Phys., 3, 2025–2041, doi:10.5194/acp-3-2025-2003, 2003.

Gonçalves, W. A., Machado, L. A., and Kirstetter P. E.: Influence of biomass aerosol on precipitation over the Central Amazon: an observational study, Atmos. Chem. Phys., 15, 6789–6800, doi:10.5194/acp-15-6789-2015, 2015.

He, Q., Zhang, M., and Huang, B.: Spatio-temporal variation and impact factors analysis of satellite-based aerosol optical depth over China from 2002 to 2015, Atmos. Environ., 129, 79–90, doi: 10.1016/j.atmosenv.2016.01.002, 2016.

Huang, R. J., Zhang, Y., Bozzetti, C., Ho, K. F., Cao, J. J., Han, Y. M., Daellenbach, K. R., Slowik, J. G., Platt, S. M., Canonaco, F., Zotter, P., Wolf, R., Pieber, S. M., Bruns, E. A., Crippa, M., Ciarelli, G., Piazzalunga, A., Schwikowski, M., Abbaszade, G., Schnelle-Kreis, J., Zimmermann, R., An, Z. S., Szidat, S., Baltensperger, U., Haddad, I. E., and Prévôt A. S.: High secondary aerosol contribution to particulate pollution during haze events in China, Nature, 514, 218–222, doi:10.1038/nature13774, 2014.

Lau, K. M. and Kim, K. M.: Observational relationships between aerosol and Asian monsoon rainfall, and circulation, Geophys. Res. Lett., 33, L21810, doi: 10.1029/2006gl027546, 2006.

Lee, K. and Chung, C. E.: Observationally constrained estimates of global fine-mode AOD, Atmos. Chem. Phys., 13, 2907–2921, doi:10.5194/acp-13-2907-2013, 2013.

Lee, K. H., Li, Z., Wong, M. S., Xin, J. Y., Wang, Y. S., Hao, W. M., and Zhao, F. S.: Aerosol single scattering albedo estimated across China from a combination of ground and satellite measurements, J. Geophys. Res. -Atmos., 112, D22S15, doi:10.1029/2007jd009077, 2007.

Li, L. and Wang, Y.: What drives the aerosol distribution in Guangdong-the most developed province in Southern China? Sci. Rep., 4, 5972, doi:10.1038/srep05972, 2014.

Li, Z., Lau, W. K., Ramanathan, V., Wu, G., Ding, Y., Manoj, M. G., Liu, J., Qian, Y., Li, J., Zhou, T., Fan, J., Rosenfeld, D., Ming, Y., Wang, Y., Huang, J., Wang, B., Xu, X., Lee, S. S., Cribb, M., Zhang, F., Yang, X., Takemura, T., Wang, K., Xia, X., Yin, Y., Zhang, H., Guo, J., Zhai, P. M., Sugimoto, N., Babu, S. S., and Brasseur, G. P.: Aerosol and monsoon climate interactions over Asia, Rev. Geophys., 54, doi:10.1002/2015rg000500, 2016.

Lin, J. T., Pan, D., and Zhang, R. X.: Trend and interannual variability of Chinese air pollution since 2000 in association with socioeconomic development: a brief overview, Atmos. Oceanic Sci. Lett., 6, 84–89, 2013.

Ricchiazzi, P., Yang, S., Gautier, C., and Sowle, D.: SBDART: A research and teaching software tool for plane-parallel radiative transfer in the Earth's atmosphere, Bull. Am. Meteorol. Soc., 79, 2101–2114, doi:10.1175/1520-0477(1998)079<2101:SARATS>2.0.CO;2, 1998.

Song, G. N., Yang, X. Y., and Fu, J. P: Aerosol optical parameter observations in Lanzhou City, J. Lanzhou University (Natural Sciences), 49, 470–483 (in Chinese), doi:10.13885/j.issn.0455-2059.2013.04.004, 2013.

Tesfaye, M., Botai, J., Sivakumar, V., and Tsidu, G. M.: Simulation of biomass burning aerosols mass distributions and their direct and semi-direct effects over south africa using a regional climate model, Meteorl. Atmos. Phys., 125(3), 177–195, doi:10.1007/s00703-014-0328-2, 2014.

Wang, H. J., Chen, H. P., and Liu, J.: Arctic sea ice decline intensified haze pollution in eastern China, Atmos. Oceanic Sci. Lett., 8, 1–9, doi:10.3878/aosl20140081, 2015.

Wang, Y., Khalizov, A., Levy, M., Zhang, R.: New directions: light absorbing aerosols and their atmospheric impacts, Atmos. Environ., 81, 713–715, doi: 10.1016/j.atmosenv.2013.09.034, 2013.

Wang, Y. Q., Zhang, X. Y., Sun, J. Y., Zhang, X. C., Che, H. Z., and Li, Y.: Spatial and temporal variations of the concentrations of PM10, PM2.5 and PM1 in China, Atmos. Chem. Phys., 15, 13585–13598, doi:10.5194/acp-15-13585-2015, 2015.

Welton, E. J., Voss, K. J., Gordon, H. R., Maring, H., Smirnov, A., Holben, B., Schmid, B., Livingston, J. M., Russell, P. B., Durkee, P. A., Formenti, P., and Andreae, M. O.: Ground-based lidar measurements of aerosols during ACE-2: instrument description, results, and comparisons with other ground-based and airborne measurements, Tellus, 52, 636–651, doi: 10.1034/j.1600-0889.2000.00025.x, 2000.

Wendisch M., Hellmuth, O., Ansmann, A., Heintzenberg, J., Engelmann, R., Althausen, D., Eichler, H., Müller, D., Hu, M., Zhang, Y., and Mao J.: Radiative and dynamic effects of absorbing aerosol particles over the Pearl River Delta, China, Atmos. Environ., 42, 6405–6416, doi: 10.1016/j.atmosenv.2008.02.033, 2008.

Wu, G. X., Li, Z. Q., Fu, C. B., Zhang, X. Y., Zhang, R. Y., Zhang, R. H., Zhou, T. J., Li, J. P., Li, J. D., Zhou, D. G., Wu, L., Zhou, L. T., He, B., and Huang, R. H.: Advances in studying interactions between aerosols and monsoon in China, Sci. China: Earth Sci., 59, 1–16, doi: 10.1007/s11430-015-5198-z, 2016.

Xia, X. A., Li, Z. Q., Holben, B., Wang, P. C., Eck, T., Chen, H. B., Cribb, M., and Zhao, Y. X.: Aerosol optical properties and radiative effects in the Yangtze Delta region of China, J. Geophys. Res., 112, d22s12, doi:10.1029/2007JD008859, 2007.

Yin, P., Brauer, M., Cohen, A., Burnett, R., Liu, J. M., Liu, Y. N., Zhou, and M. G.: Ambient fine particulate matter exposure and cardiovascular mortality in China: a prospective cohort study, The Lancet, 386, S6, doi: 10.1016/S0140-6736(15)00584-X, 2015.

Zhang, J. and Reid, J. S.: A decadal regional and global trend analysis of the aerosol optical depth using a data-assimilation grade over-water MODIS and Level 2 MISR aerosol products, Atmos. Chem. Phys., 10, 10949–10963, doi:10.5194/acp-10-10949-2010, 2010.

Zhang, Y., Fu, R., Yu, H. B., Dickinson, R. E., Juarez, R. N., Chin, M., and Wang, H.: A regional climate model study of how biomass burning aerosol impacts land-atmosphere interactions over the Amazon, J. Geophys. Res. Atmos., 113, d14s15, doi:10.1029/2007jd009449, 2008.

Zhao, S., Tie, X., Cao, J., and Zhang, Q.: Impacts of mountains on black carbon aerosol under different synoptic meteorology conditions in the Guanzhong region, China, Atmos. Res., 164, 286–296, doi: 10.1016/j.atmosres.2015.05.016, 2015a.

Zhao, S., Tie, X., Cao, J., Li, N., Li, G. H., Zhang, Q., Zhu, C. S., Long, X., Li, J. D., Feng, T., and Su, X. L.: Seasonal variation and four-year trend of black carbon in the Mid-west China: the analysis of the ambient measurement and WRF-Chem modeling, Atmos. Environ., 123, 430–439, doi: 10.1016/j.atmosenv.2015.05.008, 2015b.

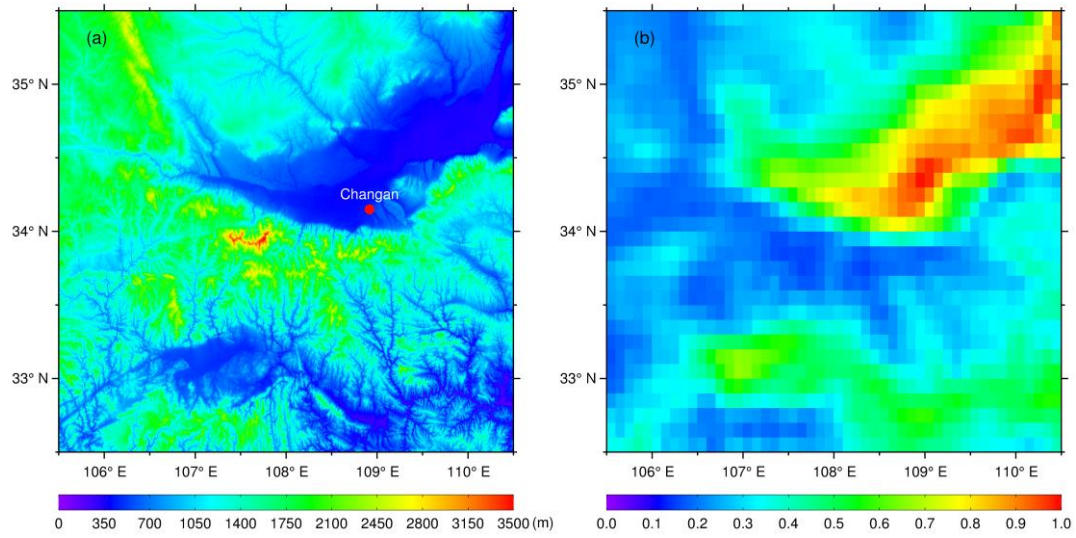

Fig. 1. (a) A topographic map of the Guan-Zhong Plain and (b) the spatial distribution of AOD over the region shown in (a). The red solid dot in (a) shows the location of the Qinling experimental site in Changan near Xi'an.

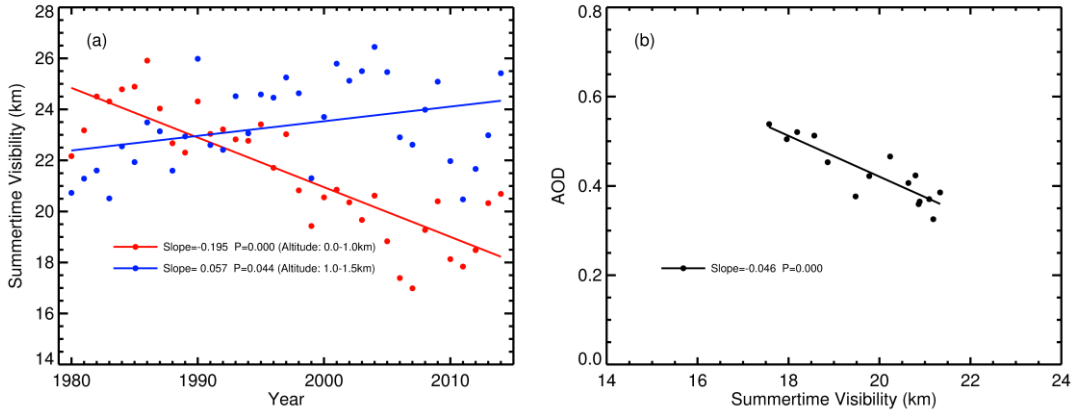

Fig. 2. (a) Long-term trends in visibility measured at meteorological stations located at different altitudes on the Guan-Zhong Plain and in the surrounding mountain region. (b) Correlation between aerosol optical depth (AOD) and visibility over the plain.

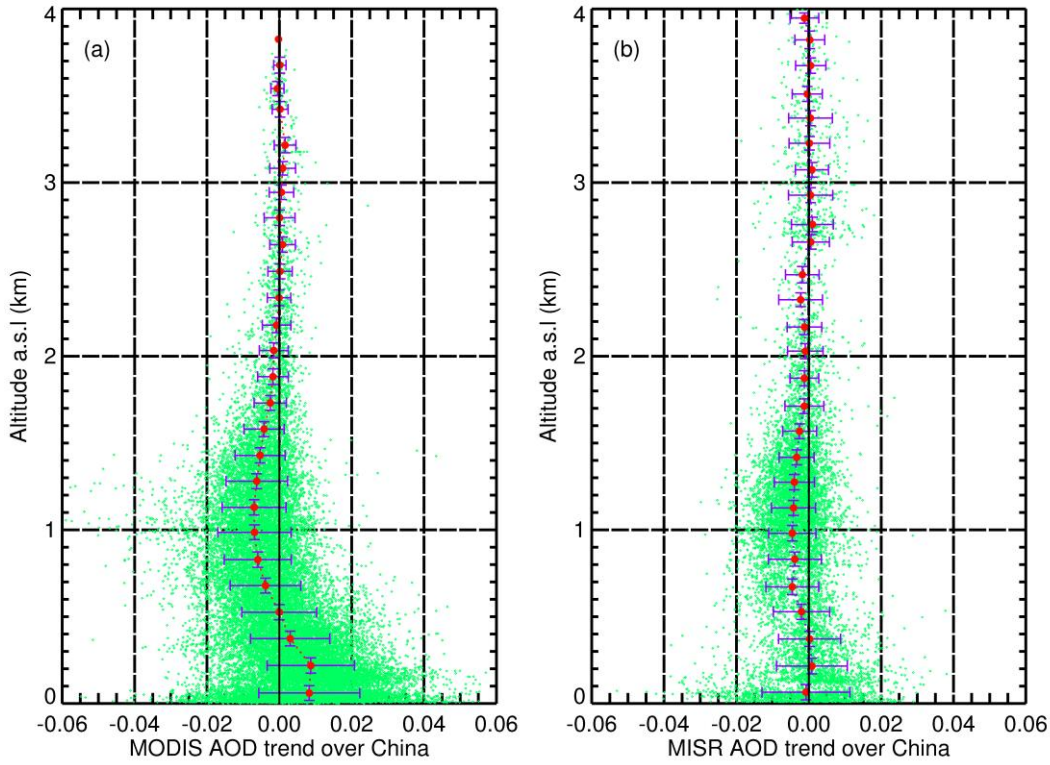

Fig. 3. Vertical profiles of aerosol optical depth (AOD) trends over the entirety of China from (a) MODIS and (b) MISR retrievals in the summer seasons of 2002 to 2014. Red dots and horizontal bars represent mean tendencies and standard deviations, respectively. The "a.s.l." in the ordinate labels stands for "above sea level". The specific region of study can be found in Fig. S2.

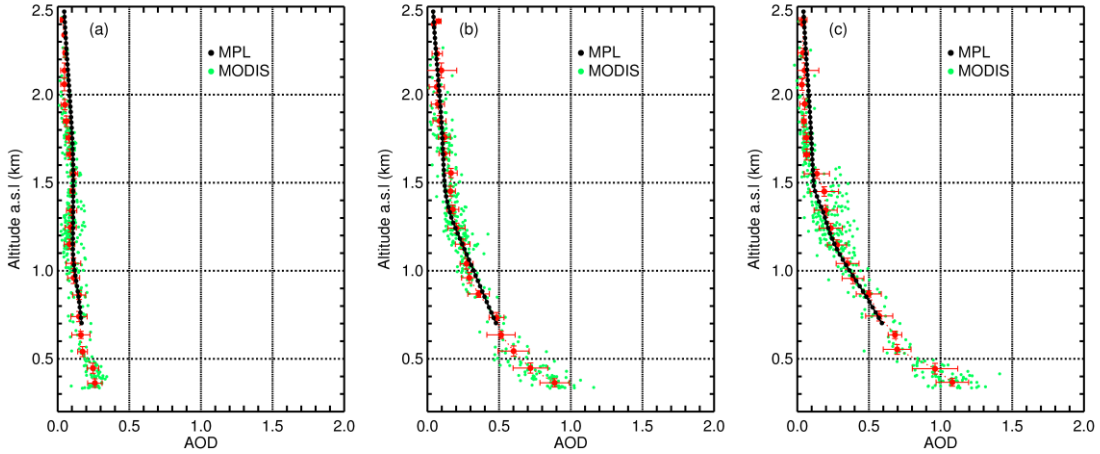

Fig. 4. AOD at different altitudes derived from MODIS retrievals over the study region shown in Fig. 1a (green dots) and MPL (black dots) data on (a) 13 September 2013 at 0600 Coordinated Universal Time (UTC), (b) 26 March 2014 at 0550 UTC, and (c) 29 September 2013 at 0600 UTC. Red dots and horizontal bars represent mean MODIS AODs and standard deviations, respectively. Only those MODIS five-minute granules with a sufficient amount of valid AOD data (> 75%) are chosen.

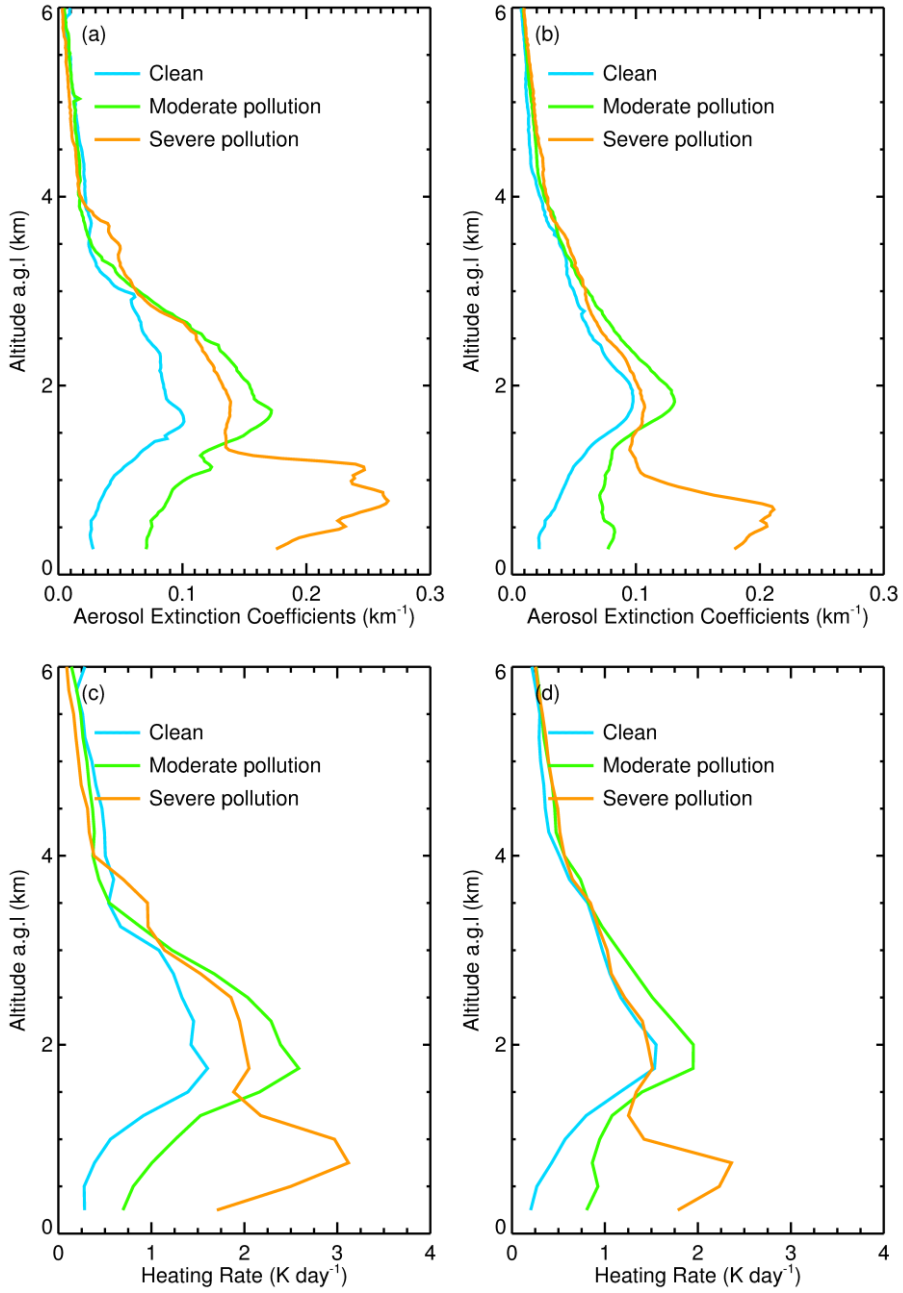

Fig. 5. Mean summertime aerosol extinction profiles measured by the MPL in (a) 2013 and (b) 2014, and summertime atmospheric heating rates induced by aerosols in (c) 2013 and (d) 2014. Profiles representing relatively clean, moderate pollution, and severe pollution scenarios are shown as blue, green, and yellow lines, respectively. The "a.g.l." in the ordinate labels stands for "above ground level".

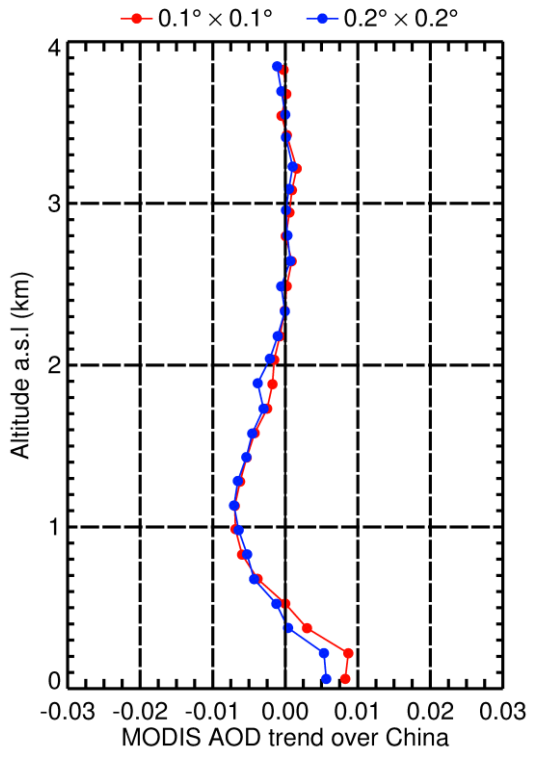

Fig. 6. Vertical profiles of aerosol optical depth (AOD) trends over the entirety of China from gridded MODIS AOD data at 0.1°×0.1° (red dots and red line) and 0.2°×0.2° (blue dots and blue line) spatial resolutions from 2002 to 2014.

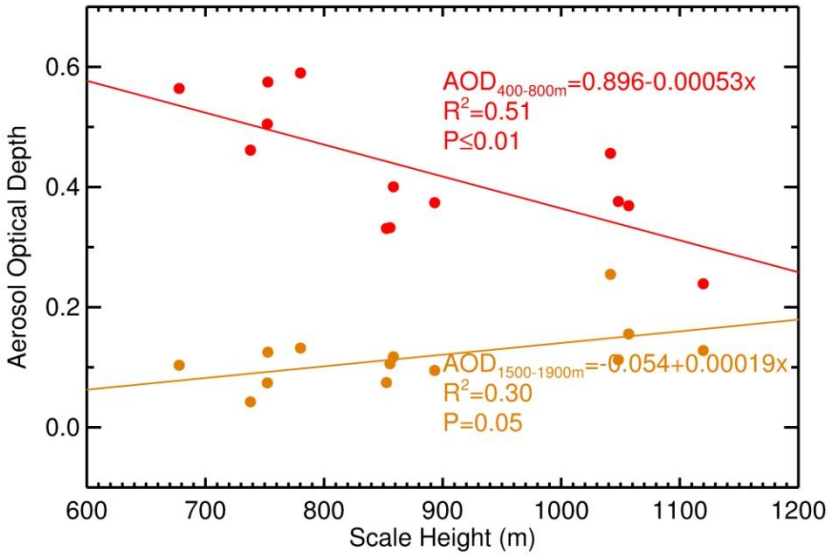

Fig. 7~~6~~. AOD in the lower PBL ($AOD_{400\text{-}800m}$) and in the upper PBL ($AOD_{1500\text{-}1900m}$) as a function of aerosol scale height. Linear-fit equations, coefficients of determination, and p-values are given.

5

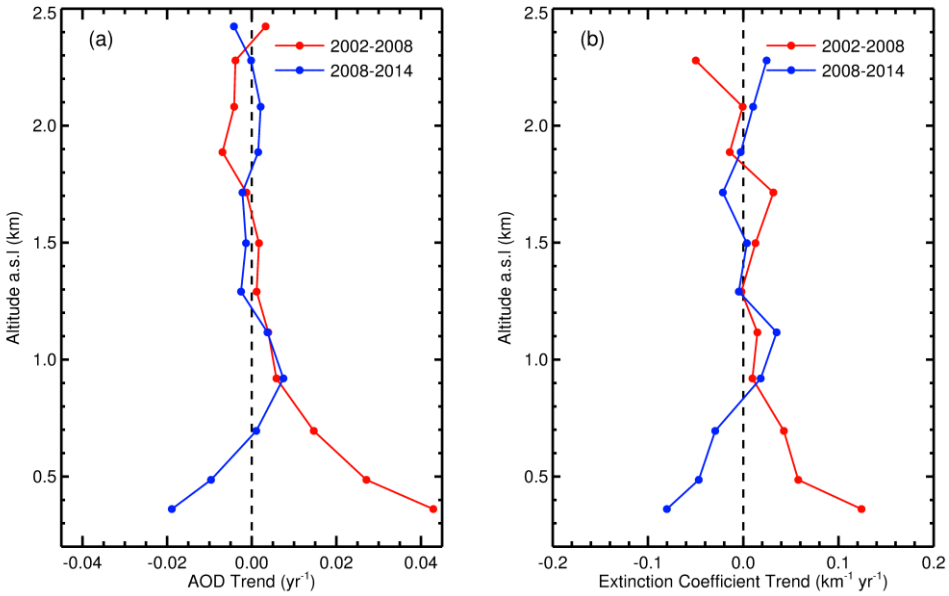

Fig. 8~~7~~. Vertical distributions of trends in summertime mean (a) AOD and (b) aerosol extinction coefficient. The vertical resolution is 200 m. Red and blue lines represent tendencies during the period 2002–2008 and 2008–2014, respectively. The "a.s.l." in the ordinate labels stands for "above sea level".

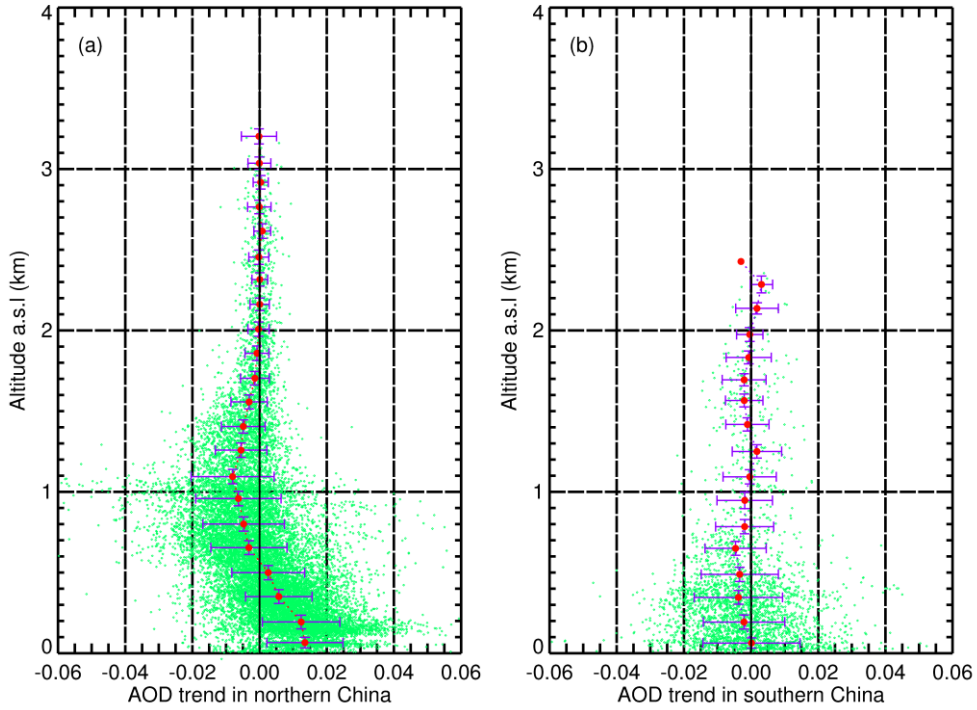

Fig. ~~9~~8. Vertical distributions of the trend in AOD from MODIS-Aqua in (a) northern (> 40°N) and (b) southern (< 30°N) China from 2002 to 2014. The specific region of study can be found in Fig. S3.

5

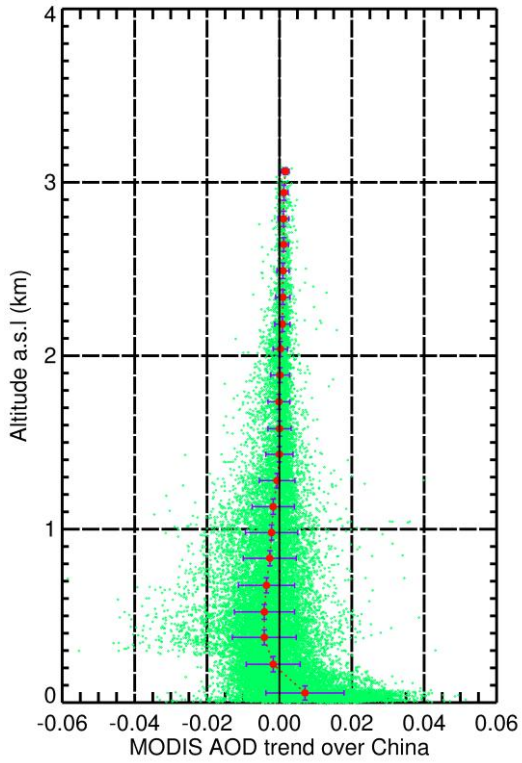

Fig. 10. Vertical profiles of the trend in aerosol optical depth (AOD) from MODIS-Aqua in the winter seasons of 2002 to 2014 over the entirety of China. The "a.s.l" in the ordinate labels stands for "above sea level".